
Classifying Overlapping Gaussian Mixtures in High Dimensions: From Optimal Classifiers to Neural Nets

Khen Cohen*, **Yaron Oz**

Raymond and Beverly Sackler School of Physics and Astronomy
Tel-Aviv University
Tel-Aviv 69978, Israel
khencohen@mail.tau.ac.il

Noam Levi*

École Polytechnique Fédérale de Lausanne (EPFL)
Switzerland
noam.levi@epfl.ch

Abstract

We derive closed-form expressions for the Bayes optimal decision boundaries in binary classification of high dimensional overlapping Gaussian mixture model (GMM) data, and show how they depend on the eigenstructure of the class covariances, for particularly interesting structured data. We empirically demonstrate, through experiments on synthetic GMMs inspired by real-world data, that deep neural networks trained for classification, learn predictors which approximate the derived optimal classifiers. We further extend our study to networks trained on authentic data, observing that decision thresholds correlate with the covariance eigenvectors rather than the eigenvalues, mirroring our GMM analysis. This provides theoretical insights regarding neural networks' ability to perform probabilistic inference and distill statistical patterns from intricate distributions.

1 Introduction

There is a well-accepted understanding in machine learning that inherent correlations or statistical structure within the data play a crucial role in enabling effective modeling. The presence of structure in the data provides important context that machine learning algorithms can leverage for accurate and meaningful knowledge extraction and generalization. Harnessing any inherent structure is widely seen as an important factor for achieving successful learning outcomes.

Determining the characteristics of natural datasets that contribute to effective training and good generalization has tremendous theoretical and practical significance. Regrettably, real-world datasets are typically viewed as samples drawn from some unknown, intricate, high-dimensional underlying population, rendering analyses that depend on accurately modeling the true distribution enormously challenging. Connecting properties of the data to learning outcomes is difficult because real data does not readily yield its generative process or population distribution.

While fully characterizing natural data distributions remains difficult, progress can still be made by considering simplified models that capture key aspects of the true distribution. One approach is to model the data via the moment expansion of the underlying population. For a random vector $X \in \mathbb{R}^d$ representing a single sample, its distribution can be described by the moment generating

*Equal Contribution

function $M_X(t) = \sum_{n=0}^{\infty} t^n \mathbb{E}(X^n)/n!$. Approximating this by retaining a finite number of moments provides a tractable model of the data distribution.

A simple starting point is the Gaussian model, which posits that a dataset’s statistical properties can be fully captured by its first two moments - the mean vector and sample covariance matrix. This assumes higher-order dependencies are negligible such that the distribution is characterized solely by its first and second central statistical moments.

In the last decade, analyzing the behavior of machine learning algorithms on idealized i.i.d. Gaussian datasets has emerged as an important area of research in high-dimensional statistics [Donoho and Tanner, 2009, Korada and Montanari, 2011, Monajemi et al., 2013, Candès et al., 2020, Bartlett et al., 2020]. Studying these simplified synthetic distributions has provided valuable insights, such as neural network scaling laws [Maloney et al., 2022, Kaplan et al., 2020], universal convergence properties [Seddik et al., 2020] and an improved understanding of the "Double Descent" phenomenon [Montanari and Saeed, 2022]. Examining learning on Gaussian approximations of real data distributions has helped establish foundational understandings of algorithmic behavior in high-dimensional settings.

A particular case of interest is that of data which is divided into a set number of classes. In certain instances, the data can be described by a mixture model, where each sample is generated separately for each class. The simplest example of such distributions is that of a Gaussian Mixture Model (GMM), on which we focus in this work.

Gaussian mixtures are a popular model in high-dimensional statistics since, besides being an universal approximator, they often lead to mathematically tractable problems. Indeed, a recent line of work has analyzed the asymptotic performance of a large class of machine learning problems in the proportional high-dimensional limit under the Gaussian mixture data assumption, see e.g. Mai and Liao [2019], Mignacco et al. [2020a], Taheri et al. [2020], Kini and Thrampoulidis [2021], Wang and Thrampoulidis [2021], Refinetti et al. [2021], Loureiro et al. [2021a].

In light of the insights gained by studying the *unsupervised*, perspective on GMM classification, we focus here on a complementary direction. Namely, we consider the *supervised* setting, where a single neural network is trained on a dataset generated from a GMM, to perform binary classification where the true labels are given. To connect the GMM with real-world data, we restrict ourselves to the case of strictly non-linearly separable GMMs, such that the class means difference is negligible compared to the class covariance difference. We refer to this setup as *overlapping GMM classification*.

Our **main contributions** are as follows:

- In Sec. 3, we derive the Bayes Optimal Classifiers (BOCs) and decision boundaries for overlapping GMM classification problems, both in the population and the empirical limits.
- In Sec. 4, under the assumptions of correlated features and Haar distributed eigenvectors, we are able to provide approximate closed form equations for the decision boundaries and discriminator distributions, as a function of the eigenvalues and eigenvectors of the different class covariances.
- In Sec. 5, we present empirical evidence, demonstrating that some networks trained to perform binary classification on a GMM, approximate the BOC. We further relate these observations to existing results, namely convergence of homogeneous networks to a KKT point.
- In Sec. 6, we demonstrate empirically that for high dimensional data, the covariance eigenvectors and not the eigenvalues determine the classification threshold for deep neural networks trained on real-world datasets, and provide an explanation inspired by our results on GMMs. In Sec. 7 we summarize our conclusions and outlook.

2 Background and Related Work

There has been significant work aimed at understanding the classification capabilities of Gaussian mixture models (GMMs), that is, recovering the cluster label for each data point rather than using labels provided by a teacher. For binary classification problems, examples include methods proposed by Mai et al. [2019], Mignacco et al. [2020b], and Deng et al. [2022], with the latter also demonstrating an equivalence between classification and single-index models. In multi-class settings, [Thrampoulidis et al., 2020] analyzed the performance of ridge regression classifiers. The most general results in this area are from Gaussian Mix Group [Loureiro et al., 2021b], which considers the use of GMMs with any convex loss function for classification. Additional results regarding kernels and GMMs include [Couillet et al., 2018, Liao and Couillet, 2019, Kammoun and Couillet, 2023, Refinetti et al., 2021], precise asymptotics [Loureiro et al., 2021c] and the connection between GMMs and real-world

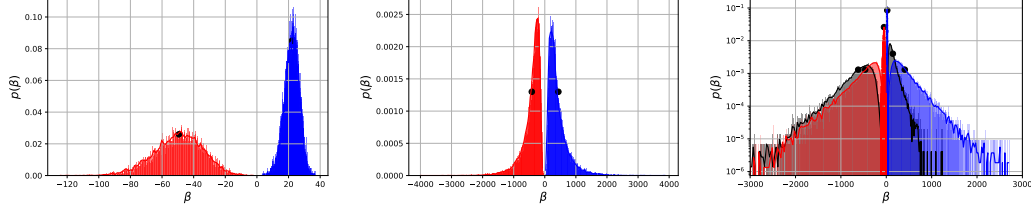


Figure 1: Probability density function of $\beta(x)$, evaluated on GMMs with different class covariance matrices. **Blue** and **red** bins indicate samples drawn from the classes A and B , respectively. Solid curves represent the numerical evaluation of Eq. (3) as a generalized χ^2 distribution. Dots indicate the values given by Eq. (5), as well as by Eq. (9). **Left:** β distribution for covariances with the same basis but different spectra. **Center:** β distribution for covariances with the same spectrum but different random bases. **Right:** β distribution comparison for covariances with both different spectra and different bases, shown in **gray**. Here, we take $\alpha_A = 0.5$, $\Delta\alpha = -0.3$, $d = 100$.

vision data [Ingrosso and Goldt, 2022]. Additionally, work has been done to understand Quadratic Discriminant Analysis (QDA) in high dimensions [Elkhalil et al., 2017, Ghogh and Crowley, 2019, Das and Geisler, 2021], which we rely heavily upon in this work.

3 Overlapping Gaussian Mixtures in High Dimensions

Consider the task of performing binary classification on samples drawn from a two class GMM, where the underlying Gaussian distributions have similar means but different covariance matrices. We generate two datasets $\mathcal{D}_A, \mathcal{D}_B$ of equal size N , and the same data dimensions $x \in \mathbb{R}^d$. Here, each sample vector is drawn from a jointly normal distribution, either $x \sim \mathcal{N}(\mu_A, \Sigma_A)$ or $x \sim \mathcal{N}(\mu_B, \Sigma_B)$, where the two means and covariance matrices distinguish between the two classes. In this setup, we assign a label value $y = 1$ to samples drawn from class A and $y = -1$ for the B class samples. Throughout this work, we consider the large number of features and large number of samples limit $d, N \rightarrow \infty$, while the ratio $d/N = \gamma \in \mathbb{R}^+$ is constant. We denote $\gamma \rightarrow 0$ as the *population* limit, while $\gamma \rightarrow 1$ as the *empirical* limit.

In the following sections, we discuss the optimal classifiers obtained first from the population and then the empirical data distributions. We then apply our results to a simplified model dataset which captures some of the properties of real-world datasets, and distinguish the roles of the covariance eigenvectors and eigenvalues for this case.

3.1 Optimal Classification on Population Data

The Bayes-optimal classifier (BOC) assigns each sample to the class that maximizes the expected value gain or its logarithm defined as

$$G(X = x) = \arg \max_{Y=y} p(X = x|Y = y)p(Y = y) = \arg \max_{Y=y} \log(p_{X|Y}) = \arg \max_{Y=y} \beta_Y, \quad (1)$$

where $p(Y = y) = 1/C$ is the class density with C the number of classes in the case of a balanced dataset. Here, $p(X = x|Y = y) = \exp(\beta_Y)$ is the conditional in-class density. The decision boundary between any two classes $y, y' \in C$ is given when $\beta_{Y=y}(X = x) = \beta_{Y=y'}(X = x)$, where the probabilities of a sample being classified as y or y' are equal. For a two-class GMM, this is obtained by simply equating the class conditional probability densities, i.e., $p_A = p_B$, leading to the *quadratic* decision rule, derived in Elkhalil et al. [2017] as well as Das and Geisler [2021], to pick class A if

$$\beta(x) = \frac{1}{2}(x^T Q x - 2q^T x + c) > 0, \quad Q = (\Sigma_B^{-1} - \Sigma_A^{-1}), \quad q = (\Sigma_B^{-1} \mu_B - \Sigma_A^{-1} \mu_A), \quad (2)$$

$$c = \mu_B^T \Sigma_B^{-1} \mu_B - \mu_A^T \Sigma_A^{-1} \mu_A - \log \left(\frac{|\Sigma_A|}{|\Sigma_B|} \right),$$

where $|O|$ is the determinant of the matrix O . This quadratic $\beta(x)$ is the Bayes classifier, or the Bayes decision variable that, when compared to zero, maximizes expected gain.

Note that the $q^T x$ term in Eq. (2) determines the *linear* decision boundary, while $x^T Q x$ determines the *nonlinear* part. For the rest of this work, we consider the **nonlinear, overlapping mixture configuration**, where $\mu_A = \mu_B = \mu$, while $\Sigma_A \neq \Sigma_B$, as a proxy for the behavior of many real world datasets [Schilling et al., 2021]. Without loss of generality, we may set $\mu = 0$, since we can

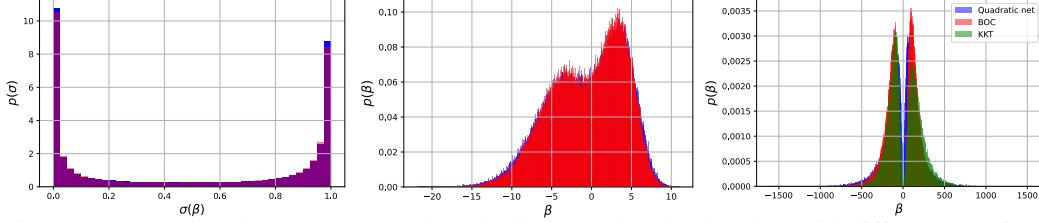


Figure 2: Comparison between BOC and quadratic network trained on data with different covariance spectrum. **Left:** accuracy, measured as the sigmoid function acting on the network/BOC output. **Center:** network/BOC output distribution. **Blue** indicates network results while **red** is the BOC prediction. Here, the network is trained with $d_h = 100$ and $N = 200k$ to 91.27% training accuracy and reaches 91.1% with $\alpha_A = 0.2$ and $\alpha_B = 0.3$. **Right:** Results for KKT convergence of a quadratic NN trained on an $\alpha = 0.2$ correlated GMM, where the class covariances share the same spectrum but are given a different random basis. **Red** indicates the BOC prediction, **blue** is the quadratic network output before the softmax function, when trained with $d_h = 100$, and **green** are the KKT predictions with $\lambda_a \propto 1/N$ and $d_h = 100$. The data dimensions are similar to the main text, i.e., $d = 100$, using $N = 100k$ samples, the network reached 100% training and 99.9% test accuracy.

always shift away the mean of the distributions, resulting in the simpler form of $\beta(x)$

$$\beta(x) = \frac{1}{2}(x^T Q x + c) = \frac{1}{2}(\text{Tr}(Q x x^T) + c) = \frac{1}{2} \sum_i q_i \tilde{\chi}_1^2 - \frac{a}{2}, \quad (3)$$

where the last transition in Eq. (3) is valid since β is given by a sum of χ^2 distributed random variables, known as the generalized chi-squared distribution [Das and Geisler, 2021], where $a \sim \mathcal{N}(\log(|\Sigma_B^{-1} \Sigma_A|), 0)$, q_i are the eigenvalues of $\Sigma_Y^{1/2} Q \Sigma_Y^{1/2}$, and $Y = A, B$. The probability density function (PDF) of β does not have a closed analytic form, but can be obtained numerically by various methods [Ferrari, 2019, Das and Geisler, 2021]. In Fig. 1, we show the β -distribution for high-dimensional Gaussian data with different covariances, obtained both empirically from Eq. (3) and by drawing from a sum of χ^2 variables matching Eq. (3).

While the full PDF of β cannot be written in a simple form, the empirical expectation value on a given set of measurements can be derived. Namely, given a set of N samples $x_i, i = 1, \dots, N$, taken from a normal distribution $\mathcal{N}(0, M)$, $M \in \mathbb{R}^{d \times d}$, the expectation value of the Bayes classifier β on these samples is simply

$$\langle \beta_M \rangle = \frac{1}{2} [\text{Tr}(QM) - \log(|\Sigma_B^{-1} \Sigma_A|)], \quad (4)$$

where $\langle \cdot \rangle$ indicates averaging over the data distribution. It can be used to define what it means for a sample to belong to class A or B , by computing the average distance between the expectation value of β on any dataset and the class values, given by

$$\langle \beta_A \rangle = -d + \text{Tr}(\Sigma_B^{-1} \Sigma_A) + c > 0, \quad \langle \beta_B \rangle = d - \text{Tr}(\Sigma_A^{-1} \Sigma_B) + c < 0, \quad (5)$$

where we averaged over $N \rightarrow \infty$ samples from the A, B distributions, and $c = -\log(|\Sigma_B^{-1} \Sigma_A|)$. We show these values as black dots in Fig. 1.

3.2 Empirical Optimal Classification

So far, we have assumed that we have access to the population covariances Σ_A, Σ_B . Here, we comment on the classification problem changes when relaxing this assumption and consider the empirical covariances which are obtained at finite dimension to sample number ratio $\gamma = \text{const}$.

In particular, we consider the case where we have access only to finitely sampled versions of the population moments, but have infinitely many samples of this noisy distribution. Here, the distributions in question for classes A, B are still gaussian, but their respective moments are not the population ones, implying that the BOC is deformed. The covariance matrices we have access to are given by measurements, that define the empirical covariances for each class $\Sigma_{N,Y} = \frac{1}{N} X_Y X_Y^T \simeq \Sigma_Y + \sqrt{\gamma} R_Y$, where $X_Y \in \mathbb{R}^{d \times N}$ is the design matrix, and R_Y is a random matrix with $\mathcal{O}(1)$

eigenvalues [Biroli and Mézard, 2023]². We can therefore rewrite the empirical BOC as

$$\beta_N(x) \simeq \frac{x^T(Q_N)x}{2} + \frac{c_N}{2}, \quad Q_N \simeq Q + \sqrt{\gamma}(R_B - R_A), \quad c_N = c - \log \left(\frac{|\mathbb{I} + \sqrt{\gamma}\Sigma_B R_B|}{|\mathbb{I} + \sqrt{\gamma}\Sigma_A R_A|} \right), \quad (6)$$

where we expand to leading order in $\gamma = \frac{d}{N}$. This implies that the empirical β_N distribution remains a generalized χ^2 with the substitution of coefficients to be the eigenvalues of $\Sigma_Y^{1/2} Q_N \Sigma_Y^{1/2}$ and the constant c is shifted by the log term. Therefore, the empirical deviation from the BOC $\Delta\beta_N = \|\beta_N - \beta\|$ is estimated by

$$\Delta\beta_N \simeq \sqrt{\gamma} |\text{Tr}(R_B(xx^T - \Sigma_B) - R_A(xx^T - \Sigma_A))|, \quad (7)$$

which decreases with $\sqrt{\gamma}$. This setting is exhibited in Fig. 1, which is meant to mimic the real-world setting, where we do not have access to the population covariance, and we can only estimate how close the empirical moments are to the population ones.

4 Analysis for a Toy Model of Complex Data

In order to connect the BOC with real world classification tasks, we focus on a specific modeling of natural data. Here, we consider a simple model of a correlated GMM inspired by the neural scaling law literature [Maloney et al., 2022, Montanari and Saeed, 2022, Levi and Oz, 2023a] as well as the signal recovery literature [Loureiro et al., 2021d, 2022]. Concretely, we assume a power law scaling spectrum, and a different basis matrix for each class

$$\Lambda_{Y,ij} = i^{-1-\alpha_Y} \delta_{ij}, \quad \Sigma_Y = O_Y^T \Lambda O_Y, \quad (8)$$

where δ_{ij} is the d dimensional identity matrix and O_Y is a random orthogonal matrix. In the following sections, we distinguish the role of eigenvalues and eigenvectors in determining the BOC for overlapping GMMs.

4.1 Diagonal Correlated Covariances

As a first example, we consider the case where Σ_A, Σ_B are both diagonal matrices with different eigenvalues, such that $O_A = O_B = \mathbb{I}$, and $\Sigma_A = \Lambda_A, \Sigma_B = \Lambda_B$. Given a model of power law scaling dataset A with α_A , we can define the power law exponent of the dataset B to be $\alpha_B = \alpha_A + \Delta\alpha$. Here, we can obtain explicit expressions for β as

$$\langle\beta_A\rangle = \frac{1}{2} \left(H_d^{(-\Delta\alpha)} - d - \Delta\alpha \log(\Gamma(d+1)) \right), \quad \langle\beta_B\rangle = \frac{1}{2} \left(d - H_d^{(\Delta\alpha)} - \Delta\alpha \log(\Gamma(d+1)) \right), \quad (9)$$

where H_d^i is the Harmonic number, and $\Gamma(x)$ is the Gamma function. In the limit of $d \rightarrow \infty$, one obtains that $\langle\beta_A\rangle \propto \frac{1}{4} \left(2d \left(\frac{d^{\Delta\alpha}}{\Delta\alpha+1} - 1 \right) - (2d\Delta\alpha + \Delta\alpha) \log(d) \right)$ at leading order. This is a rapidly growing function in d , showing that even a small difference in spectra can be magnified simply by dimensionality, leading to correct classification.

4.2 Rotated Correlated Covariances

Next, we consider the case where Σ_A, Σ_B share the same spectrum, but are rotated with respect to one another, such that $\Sigma_A = O_A^T \Lambda O_A, \Sigma_B = O_B^T \Lambda O_B$. The sample expectation for the BOC reads

$$\langle\beta_A\rangle = -\langle\beta_B\rangle = \frac{1}{2} \left(\text{Tr}(O^T \Lambda^{-1} O \Lambda) - d \right), \quad (10)$$

where $O = O_A O_B^T$ is itself a random orthogonal matrix. In the limit of $d \rightarrow \infty$, we may replace the expectation value over the dataset with its integral with respect to the Haar measure on the rotation group, and obtain a closed form expression as

$$\langle\beta_A\rangle_O = \frac{1}{2} \left[\frac{1}{d} \text{Tr}(\Lambda^{-1}) \text{Tr}(\Lambda) - d \right] = \frac{1}{2} \left(\frac{H_d^{(-1-\alpha)} H_d^{(1+\alpha)}}{d} - d \right), \quad (11)$$

where the final expression is given for a power law scaling dataset. In the limit of $d \rightarrow \infty$, Eq. (11) grows as $\langle\beta_A\rangle_O \propto \frac{1}{2} \left(\frac{1}{\alpha(\alpha+2)} + 1 \right) d - \frac{d^{\alpha+1} \zeta(\alpha+1)}{2(\alpha+2)}$, which is a faster growing function than Eq. (9)

²This result holds in the limit of $d^2 \ll N$. In the case of $d \ll N$, Q_N is a Wishart matrix, which requires more careful treatment such as given in Liao and Couillet [2019], Tiomoko et al. [2019], Zhang et al. [2018], which we leave for future work.

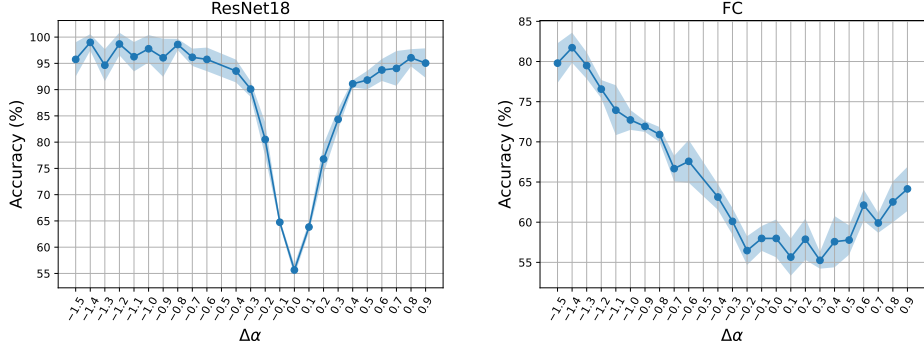


Figure 3: Two Gaussian classification task, with the same eigenvectors but different eigenvalues bulk: the first one with $\alpha = 0.5$ and the second with $\alpha + \Delta\alpha$. The model is FC, averaged over 5 training runs - the solid line represents the mean accuracy and shaded area represents 1-sigma error bars.

for $\Delta\alpha/\alpha < 1$ indicating that it requires a large difference in the relative eigenvalue scaling exponents $\Delta\alpha/\alpha$ to shift the BOC distribution, when compared to the effect of a basis difference. We show this effect explicitly in the different panels of Fig. 1. This implies that the eigenvectors are likely to play a more significant role than eigenvalues in datasets which are well modeled by the above setup.

5 Neural Networks as Nearly Optimal Classifiers

Having established the BOC behavior on overlapping GMMs, we can now ask how these conclusions translate to the learning process in some neural network architectures. Namely, NNs have been shown to achieve optimal classification in some cases [Radhakrishnan et al., 2023]. We demonstrate that NNs quite generically approximate the quadratic BOC, and provide some intuition as to how it may occur by appealing to the directional convergence of gradient descent to a KKT point.

5.1 Neural Network Classifier

Let $\mathcal{D} = \{(\mathbf{x}_a, y_a)\}_{a=1}^N \subseteq \mathbb{R}^d \times \{-1, 1\}$ be a binary classification training dataset. Let $\Phi(\boldsymbol{\theta}; \cdot) : \mathbb{R}^d \rightarrow \mathbb{R}$ be a neural network parameterized by $\boldsymbol{\theta} \in \mathbb{R}^p$. For a loss function $\ell : \mathbb{R} \rightarrow \mathbb{R}$ the empirical loss of $\Phi(\boldsymbol{\theta}; \cdot)$ on the dataset \mathcal{D} is $\mathcal{L}(\boldsymbol{\theta}) := \sum_{a=1}^N \ell(y_a \Phi(\boldsymbol{\theta}; \mathbf{x}_a))$. We focus on the *logistic loss* (a.k.a. *binary cross entropy*), namely, $\ell(q) = \log(1 + e^{-q})$.

The network function $\Phi(\boldsymbol{\theta}; \cdot)$, can therefore be interpreted as the equivalent of the BOC variable β in the previous sections. With this intuition in mind, we expect that neural networks trained to perform binary classification should converge to the BOC, i.e., $\Phi(\boldsymbol{\theta}; \cdot) \rightarrow \beta$ with sufficient with sufficient network expressivity, number of samples and successful optimization dynamics.

The simplest network architecture that one may employ is a linear classifier, where $\Phi(z) = z$. Such linear networks of any depth cannot approximate the BOC given by Eq. (3), as it is fully nonlinear.

Next, we consider a non-trivial case, by taking a two layer network, with the activation function $\sigma(z) = z^2$, i.e. the quadratic activation. Quadratic activations are natural in the context of signal processing, where often detectors can only measure the amplitude (and not phase) of a signal, e.g. the phase retrieval problem [Jaganathan et al., 2015, Dong et al., 2023]. It has also gained in popularity recently as a prototypical non-convex optimization problem with strict saddles, e.g. Candes et al. [2014], Chen et al. [2019], Arnaboldi et al. [2024], Martin et al. [2023]. It has also been shown such two-layer blocks can be used to simulate higher-order polynomial neural networks and sigmoidal activated neural networks [Livni et al., 2014, Soltani and Hegde, 2018]. Concretely, a sufficiently expressive network function to fully realize the BOC is

$$\Phi = v^T(Wx)^2 + b = \sum_i \sum_{\mu, \nu} v_i W_{i\mu} W_{i\nu} x_\mu x_\nu + b, \quad (12)$$

where $W \in \mathbb{R}^{d_h \times d}$, $v^T \in \mathbb{R}^{d_h}$ are weight matrices at the input and hidden layers, d_h is the number of hidden units, and b is the bias at the last layer. In this setup, a predictor function can be easily matched to the BOC by matching

$$\sum_{i=1}^d v_i W_{i\mu} W_{i\nu} = \frac{1}{2} Q_{\mu\nu}, \quad b = \frac{c}{2}, \quad (13)$$

where the number of hidden neurons correspond to the minimal number required to match the rank of the BOC matrix Q , hence $d_h \geq d$. Since this network is expressive enough to fully reproduce the BOC, our analysis in Sec. 3.1 holds, and the importance of eigenvalues and eigenvectors is manifest. We show the result of a quadratic network converging to the BOC in Fig. 2 where $d = d_h = 100$.

5.2 Karush–Kuhn–Tucker (KKT) Convergence

Another source of intuition for the value of d_h may be found in the KKT convergence equation [Ji and Telgarsky, 2020, Lyu and Li, 2020], which states, in a nutshell, that the weights of a homogeneous neural network³, trained with the logistic loss for binary classification, using an infinitesimal learning rate $\eta \rightarrow 0$ and infinite iterations $t \rightarrow \infty$, will converge in direction to a KKT fixed point given by

$$\tilde{\theta} = \sum_{a=1}^N \lambda_a y_a \nabla_{\theta} \Phi(\tilde{\theta}; \mathbf{x}_a), \quad (14)$$

where $\tilde{\theta}$ are the network weights at convergence, \mathbf{x}_a are the samples and y_a are the sample labels. Here, $\lambda_a \in \mathbb{R}^+$, and are nonzero only for samples on the decision boundary. The full theorem and requirements are provided in App. B. We can apply Eq. (14) to the quadratic network as

$$\tilde{v} = \sum_{a=1}^N \lambda_a y_a (\tilde{W} x_a)^2, \quad \tilde{W} = \sum_{a=1}^N \lambda_a y_a \tilde{v}^T x_a (W x_a), \quad (15)$$

where we assume no biases (consistent with the case of similar spectrum and different basis). We posit, that in high dimensions $\lambda_a \propto N^{-1}$, since at large d every sample in the dataset should lie on the margin and contribute an equal amount, and the decision hyper-surface area should be comparable to the entire volume [Hsu et al., 2022]. Under this ansatz, the above equations can be solved numerically, and indeed approximate the BOC as d_h increases. We present evidence that the Bayes optimal decision boundary can be realized by a two-layer neural network with quadratic activation, and increasing the number of hidden units increases the probability of converging to this minima under gradient flow in Fig. 2.

6 Results Extending to Realistic Data and Networks

In the previous section, we showed that small differences in eigenvalues and eigenvectors are magnified by the dimension, making classification easier. We further demonstrated that differences in the eigenvectors are faster growing in the dimension of the data, suggesting eigenvectors play a more significant role in the Bayesian decision boundary. Next, we will provide clear evidence that these conclusions hold, and extend to real-world datasets, by performing a set of tests related to the various properties of the covariance matrices. We train two common network architectures to perform binary classification, both on GMMs and on real images, exploring their performance as we change the covariance structure of each class.

Concretely, we consider two popular network architectures: fully connected (FC) and convolutional neural networks (CNN), tested on the CIFAR10 [Krizhevsky, 2012] and Fashion-MNIST [Xiao et al., 2017] datasets. For each training procedure, the model is optimized to classify samples from two classes in the given dataset (class 0 versus classes 1-9 aggregated).

The optimization procedure proceeds as follows: for each class, the samples are split into training and evaluation subsets. We then compute the covariance matrix of the training and evaluation subsets separately for the first and second classes. New synthetic data is generated by sampling from a multivariate Gaussian distribution with zero mean and the corresponding covariance matrix. This synthetic data is used to train the model to distinguish between the two classes (i.e. classify the Gaussians). When trained on real images, the model is tested on real images and not gaussians.

The optimization objective is the binary cross-entropy loss. The FC architecture consists of 3 dense layers with 2048 units each utilizing ReLU activations, followed by a softmax output layer. For

³Homogeneity, i.e. $f(L\theta) = L^a f(\theta)$, where f is the output of the network, θ are the network parameters, and $L, a \in \mathbb{R}$, a quadratic network satisfies this requirement as it is composed of monomials.

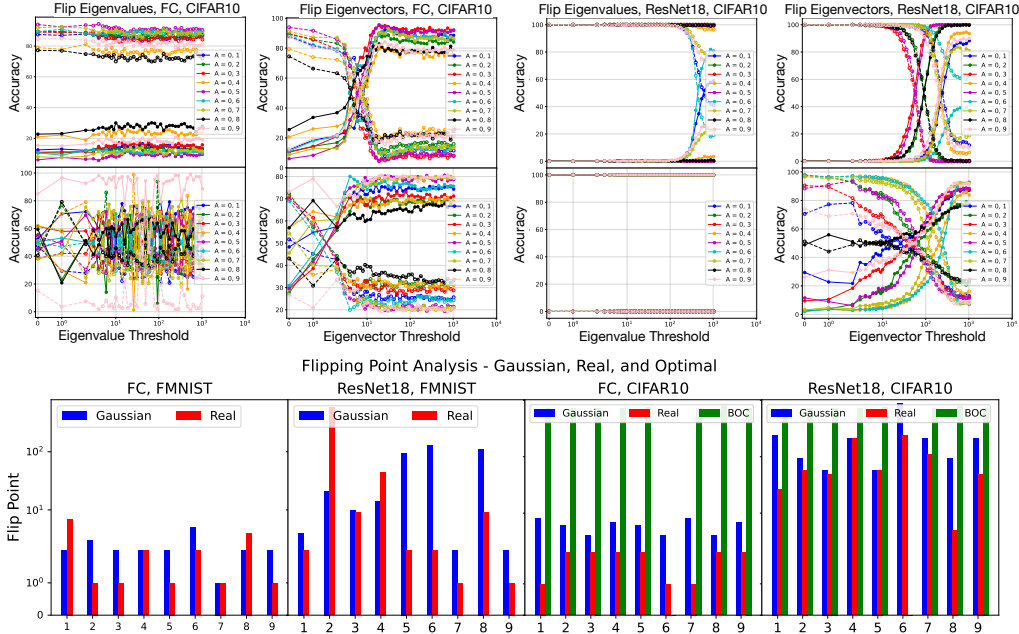


Figure 4: The classification flipping test on the FMNIST and CIFAR10 datasets between class 0 and other classes. **Top row:** training and tests on GMMs generated from the class covariance matrices. **Middle row:** training and tests on real images after whitening, rescaling and coloring. **Bottom row:** eigenvector threshold at the flipping point, for FMNIST and CIFAR10, using GMMs and real images, when either training with a NN or predicting with the BOC. **Blue** columns indicate the flipping point on GMM classification, **red** indicates the same test on real images, and **green** shows the predictions of the BOC given only by information on the covariance matrices, as given by Eq. (3). The BOC is only shown for CIFAR10, due to numerical instabilities.

CNNs, we employ ResNet-18 [He et al., 2015]. All models are optimized with the Adam optimizer, a learning rate of 0.001, and Cosine Annealing LR scheduling over 50 epochs with a batch size of 256. The synthetic datasets contain 1,280 images per class, split 80-20 for training and validation. Our computational resource was a single NVIDIA GeForce GTX 1650 GPU, with 16GB RAM.

6.1 $\Delta\alpha$ Tests on GMMs

We first perform an experiment to quantitatively evaluate a network’s ability to utilize covariance matrix eigenvalue scaling for classification tasks. Specifically, two random covariance matrices are constructed using Eq. (8), with one covariance has the spectral scaling of α and the other of $\alpha + \Delta\alpha$. Critically, both matrices share the same basis of eigenvectors. Approximately 500 samples are then drawn from each covariance matrix.

A model is trained to classify between the two classes defined by the distinct covariance matrices. Fig. 3 shows the results for a fully connected network, as well as for a ResNet18 architecture [He et al., 2015]. To assess the performance variability, the results are averaged over an ensemble of five independent training runs.

By varying only the scaling exponent between the covariances while keeping the eigenvectors fixed, this experiment protocol directly tests a network’s capability to leverage the eigenvalue scaling imparted by the covariance matrix for discriminative learning. The stability of the classifications indicate the degree to which these deep models can extract and utilize the intrinsic geometrical information encoded in the covariance descriptors.

6.2 Flip Tests on GMMs Constructed from Real Data

Next, we consider the role of eigenvectors and eigenvalues in classifying overlapping GMMs, as well as real images. It is known that the eigenvectors and eigenvalues of the data covariance matrix reveal different aspects of the data. In order to understand which of the two contains pertinent information for NN classification performance, we consider the following setup: we study two datasets, with covariance matrices C_1 and C_2 , and decompose each one of them to a set of eigenvectors and

eigenvalues: $\{\lambda_i^1, v_i^1\}, \{\lambda_i^2, v_i^2\}$. We then construct a new covariance matrix by combining some of the eigenvalues and eigenvectors of C_1 and C_2 . To quantify the ratio of eigenvectors/eigenvalues coming from each class, we define two threshold indices τ_λ for the eigenvalues and τ_v for the eigenvectors, where each of them is an integer between 0 and the dimension of C_1, C_2 , given by d . The new covariance matrix reads:

$$C_{\tau_\lambda, \tau_v} = V^T \Lambda V, \quad (16)$$

where $V = V_{\tau_v}$ and $\Lambda = \Lambda_{\tau_\lambda}$ are the new basis, and eigenvalues, respectively, which are composed by a mixture between the two classes:

$$v_i = \begin{cases} v_i^1 & i \leq \tau \\ v_i^2 & \tau < i \end{cases}, \quad \lambda_i = \begin{cases} \lambda_i^1 & i \leq \tau \\ \lambda_i^2 & \tau < i \end{cases}. \quad (17)$$

This process is denoted as a *flip test*, illustrated in Fig. 8.

It is worth noting that when composing the rotation matrix V , we must ensure that it is nearly orthogonal to maintain the properties of a true basis, which is not guaranteed in our scheme. However, we find that this matrix is very close to orthogonal in the following sense: we define the following error, and require $e \ll 1$

$$e \equiv \max_{\tau} \frac{1}{d} \|V^\dagger V - I\|_F, \quad (18)$$

where $\|\cdot\|_F$ is the Frobenius norm. Eq. (18) sets an upper bound for the error over all of the thresholds $\tau \in [0, d]$. We practically found that $e \sim 0.018$, while computing it for a randomly generated matrix composed of unit norm vectors gives $e \sim 1$.

In Fig. 4 (top row), we show the results of training a FC and ResNet18 networks to classify GMMs constructed from different C_1, C_2 and tested on samples drawn from C_{τ_λ, τ_v} . The baseline results are that the network classifies samples as coming from C_1 if C_{τ_λ, τ_v} has both the eigenvalues and eigenvectors of C_1 . When constructing C_{τ_λ, τ_v} with the eigenvectors of C_1 and the eigenvalues of C_2 , the network still classifies samples as coming from C_1 . This is not the case when taking the eigenvalues from C_1 but some of the eigenvectors from C_2 . Evidently, it requires a $\mathcal{O}(100)$ eigenvectors from C_2 to convince the network that the samples came from C_2 .

In Fig. 4 (bottom row), we show that this result is architecture dependent, but the existence of an eigenvector flipping point persists throughout our experiments. We further compare this result with the BOC prediction, showing that indeed the BOC requires more eigenvectors to be flipped before determining that samples belong in C_2 rather than C_1 . This is shown in detail in Fig. 11.

We further analyze the above flip tests for different data sizes used to construct C_1 and C_2 . We find that the results do not change above a certain number of samples, as the covariance matrices are well approximated beyond that point. Fig. 12 shows the results.

6.3 Flip Tests on Real Data

To ensure that the overlapping mixture model holds for real-data, we examined the effect of adding the vector class means computed from the CIFAR10 and FMNIST datasets. We observed no qualitative change in the results, indicating that the assumption of zero mean is justified in these cases.

In order to perform the same flipping tests on real images, we simply perform a whitening transformation, followed by a rescaling, and then rotating to the basis of choice [Belhumeur et al., 1997]. For an illustration of the resulting images see Fig. 9 and Fig. 10. This process ensures that the class covariance matrices of the data have been matched to our design, but inherently affects all the higher moments of the underlying distribution in an unpredictable way. Interestingly, as can be seen in Fig. 4 (top row), the occurrence of a clear flipping point which depends on eigenvectors and not eigenvalues is manifest in real images. In Fig. 4 (bottom row) we show a comparison between the thresholds for GMMs and real images, where the results indicate a close similarity, particularly for ResNet18 trained on CIFAR10, which can be attributed to its high expressivity.

7 Conclusions and Limitations

We studied binary classification of high dimensional overlapping GMM data as a framework to model real-world image datasets and to quantify the importance for the classification tasks of the eigenvalues and the eigenvectors of the data covariance matrix. We showed that deep neural networks trained for classification, learn predictors that approximate the Bayes optimal classifiers, and demonstrated

that the decision thresholds for networks trained on authentic data correlate with the covariance eigenvectors rather than the eigenvalues, compatible with the GMM analysis. Our results reveal new theoretical insights to the neural networks’ ability to perform probabilistic inference and distill statistical patterns from complex distributions.

Limitations: Firstly, we focused on the $\gamma \ll 1$ regime of the estimated class covariances, while in many real-world cases, the empirical limit may be more applicable Levi and Oz [2023b]. In Sec. 5.2, our ansatz neglected the dependence of λ on d/N and the spectral density, which nonlinearly determines the number of points which lie on the decision surface. It might be possible to derive a similar result to Hsu et al. [2022] by taking a feature map approach to the quadratic net, but we postpone this to future work. Finally, while we quantified the significance of the detailed structure of the data covariance matrix, i.e. its eigenvalues and eigenvectors and their relative importance for classification, we are still left with the open question regarding the relative importance of the higher moments of the distribution, which we leave for a future study.

8 Acknowledgements

We would like to thank Amir Globerson, Yohai Bar-Sinai, Yue Lu and Bruno Loureiro for useful discussions. NL would like to thank G-Research for the award of a research grant, as well as the CERN-TH department for their hospitality during various stages of this work. The work of Y.O. is supported in part by Israel Science Foundation Center of Excellence.

References

- David Donoho and Jared Tanner. Observed universality of phase transitions in high-dimensional geometry, with implications for modern data analysis and signal processing. *Philosophical Transactions of the Royal Society A: Mathematical, Physical and Engineering Sciences*, 367(1906): 4273–4293, 2009.
- Satish Babu Korada and Andrea Montanari. Applications of the lindeberg principle in communications and statistical learning. *IEEE Transactions on Information Theory*, 57(4):2440–2450, 2011. doi: 10.1109/TIT.2011.2112231.
- Hatef Monajemi, Sina Jafarpour, Matan Gavish, David L. Donoho, Sivaram Ambikasaran, Sergio Bacallado, Dinesh Bharadia, Yuxin Chen, Young Choi, Mainak Chowdhury, Soham Chowdhury, Anil Damle, Will Fithian, Georges Goetz, Logan Groseck, Sam Gross, Gage Hills, Michael Hornstein, Milinda Lakkam, Jason Lee, Jian Li, Linxi Liu, Carlos Sing-Long, Mike Marx, Akshay Mittal, Albert No, Reza Omrani, Leonid Pekelis, Junjie Qin, Kevin Raines, Ernest Ryu, Andrew Saxe, Dai Shi, Keith Siilats, David Strauss, Gary Tang, Chaojun Wang, Zoey Zhou, and Zhen Zhu. Deterministic matrices matching the compressed sensing phase transitions of gaussian random matrices. *Proceedings of the National Academy of Sciences*, 110(4):1181–1186, 2013. doi: 10.1073/pnas.1219540110.
- Emmanuel J Candès, Pragya Sur, et al. The phase transition for the existence of the maximum likelihood estimate in high-dimensional logistic regression. *The Annals of Statistics*, 48(1):27–42, 2020.
- Peter L. Bartlett, Philip M. Long, Gábor Lugosi, and Alexander Tsigler. Benign overfitting in linear regression. *Proceedings of the National Academy of Sciences*, 117(48):30063–30070, 2020. ISSN 0027-8424. doi: 10.1073/pnas.1907378117.
- Alexander Maloney, Daniel A. Roberts, and James Sully. A solvable model of neural scaling laws, 2022.
- Jared Kaplan, Sam McCandlish, Tom Henighan, Tom B. Brown, Benjamin Chess, Rewon Child, Scott Gray, Alec Radford, Jeffrey Wu, and Dario Amodei. Scaling laws for neural language models, 2020.
- Mohamed El Amine Seddik, Cosme Louart, Mohamed Tamaazousti, and Romain Couillet. Random matrix theory proves that deep learning representations of gan-data behave as gaussian mixtures, 2020.

- Andrea Montanari and Basil N. Saeed. Universality of empirical risk minimization. In *Proceedings of Thirty Fifth Conference on Learning Theory*, volume 178 of *Proceedings of Machine Learning Research*, pages 4310–4312. PMLR, 02–05 Jul 2022.
- Xiaoyi Mai and Zhenyu Liao. High-dimensional classification via empirical risk minimization: Improvements and optimality. *arXiv: 1905.13742*, 2019.
- Francesca Mignacco, Florent Krzakala, Yue Lu, Pierfrancesco Urbani, and Lenka Zdeborova. The role of regularization in classification of high-dimensional noisy gaussian mixture. In *International Conference on Machine Learning*, pages 6874–6883. PMLR, 2020a.
- Hossein Taheri, Ramtin Pedarsani, and Christos Thrampoulidis. Optimality of least-squares for classification in gaussian-mixture models. In *2020 IEEE International Symposium on Information Theory (ISIT)*, pages 2515–2520. IEEE, 2020.
- Ganesh Ramachandra Kini and Christos Thrampoulidis. Phase transitions for one-vs-one and one-vs-all linear separability in multiclass gaussian mixtures. In *ICASSP 2021-2021 IEEE International Conference on Acoustics, Speech and Signal Processing (ICASSP)*, pages 4020–4024. IEEE, 2021.
- Ke Wang and Christos Thrampoulidis. Benign overfitting in binary classification of gaussian mixtures. In *ICASSP 2021-2021 IEEE International Conference on Acoustics, Speech and Signal Processing (ICASSP)*, pages 4030–4034. IEEE, 2021.
- Maria Refinetti, Sebastian Goldt, Florent Krzakala, and Lenka Zdeborová. Classifying high-dimensional gaussian mixtures: Where kernel methods fail and neural networks succeed, 2021.
- Bruno Loureiro, Gabriele Sicuro, Cedric Gerbelot, Alessandro Pocco, Florent Krzakala, and Lenka Zdeborova. Learning gaussian mixtures with generalized linear models: Precise asymptotics in high-dimensions. In *Advances in Neural Information Processing Systems*, volume 34, pages 10144–10157, 2021a.
- Xiaoyi Mai, Zhenyu Liao, and Romain Couillet. A Large Scale Analysis of Logistic Regression: Asymptotic Performance and New Insights. In *ICASSP 2019 - 2019 IEEE International Conference on Acoustics, Speech and Signal Processing (ICASSP)*, pages 3357–3361, May 2019. doi: 10.1109/ICASSP.2019.8683376. ISSN: 2379-190X.
- Francesca Mignacco, Florent Krzakala, Yue M. Lu, and Lenka Zdeborová. The role of regularization in classification of high-dimensional noisy gaussian mixture. 2020b. doi: 10.48550/ARXIV.2002.11544. URL <https://arxiv.org/abs/2002.11544>.
- Zeyu Deng, Abla Kammoun, and Christos Thrampoulidis. A model of double descent for high-dimensional binary linear classification. *Information and Inference: A Journal of the IMA*, 11(2): 435–495, June 2022. ISSN 2049-8772. doi: 10.1093/imaiai/iaab002. URL <https://doi.org/10.1093/imaiai/iaab002>.
- Christos Thrampoulidis, Samet Oymak, and Mahdi Soltanolkotabi. Theoretical insights into multi-class classification: a high-dimensional asymptotic view. In *Proceedings of the 34th International Conference on Neural Information Processing Systems, NIPS’20*, pages 8907–8920, Red Hook, NY, USA, December 2020. Curran Associates Inc. ISBN 9781713829546.
- Bruno Loureiro, Gabriele Sicuro, Cédric Gerbelot, Alessandro Pocco, Florent Krzakala, and Lenka Zdeborová. Learning gaussian mixtures with generalised linear models: Precise asymptotics in high-dimensions. 2021b. doi: 10.48550/ARXIV.2106.03791. URL <https://arxiv.org/abs/2106.03791>.
- Romain Couillet, Zhenyu Liao, and Xiaoyi Mai. Classification asymptotics in the random matrix regime. In *2018 26th European Signal Processing Conference (EUSIPCO)*, pages 1875–1879, 2018. doi: 10.23919/EUSIPCO.2018.8553034.
- Zhenyu Liao and Romain Couillet. A large dimensional analysis of least squares support vector machines. *IEEE Transactions on Signal Processing*, 67(4):1065–1074, February 2019. ISSN 1941-0476. doi: 10.1109/tsp.2018.2889954. URL <http://dx.doi.org/10.1109/TSP.2018.2889954>.

- Abla Kammoun and Romain Couillet. Covariance discriminative power of kernel clustering methods. *Electronic Journal of Statistics*, 17(1):291 – 390, 2023. doi: 10.1214/23-EJS2107. URL <https://doi.org/10.1214/23-EJS2107>.
- Bruno Loureiro, Gabriele Sicuro, Cedric Gerbelot, Alessandro Pocco, Florent Krzakala, and Lenka Zdeborová. Learning gaussian mixtures with generalized linear models: Precise asymptotics in high-dimensions. In M. Ranzato, A. Beygelzimer, Y. Dauphin, P.S. Liang, and J. Wortman Vaughan, editors, *Advances in Neural Information Processing Systems*, volume 34, pages 10144–10157. Curran Associates, Inc., 2021c. URL https://proceedings.neurips.cc/paper_files/paper/2021/file/543e83748234f7cbab21aa0ade66565f-Paper.pdf.
- Alessandro Ingrosso and Sebastian Goldt. Data-driven emergence of convolutional structure in neural networks. *Proceedings of the National Academy of Sciences*, 119(40), September 2022. ISSN 1091-6490. doi: 10.1073/pnas.2201854119. URL <http://dx.doi.org/10.1073/pnas.2201854119>.
- Khalil Elkhilil, Abla Kammoun, Romain Couillet, Tareq Y Al-Naffouri, and Mohamed-Slim Alouini. Asymptotic performance of regularized quadratic discriminant analysis based classifiers. In *2017 IEEE 27th International Workshop on Machine Learning for Signal Processing (MLSP)*, pages 1–6. IEEE, 2017.
- Benyamin Ghogh and Mark Crowley. Linear and quadratic discriminant analysis: Tutorial, 2019.
- Abhranil Das and Wilson S. Geisler. A method to integrate and classify normal distributions. *Journal of Vision*, 21(10):1, September 2021. ISSN 1534-7362. doi: 10.1167/jov.21.10.1. URL <http://dx.doi.org/10.1167/jov.21.10.1>.
- Achim Schilling, Andreas Maier, Richard Gerum, Claus Metzner, and Patrick Krauss. Quantifying the separability of data classes in neural networks. *Neural Networks*, 139:278–293, July 2021. ISSN 0893-6080. doi: 10.1016/j.neunet.2021.03.035. URL <http://dx.doi.org/10.1016/j.neunet.2021.03.035>.
- Alberto Ferrari. A note on sum and difference of correlated chi-squared variables, 2019.
- Giulio Biroli and Marc Mézard. Generative diffusion in very large dimensions. *Journal of Statistical Mechanics: Theory and Experiment*, 2023(9):093402, September 2023. ISSN 1742-5468. doi: 10.1088/1742-5468/acf8ba. URL <http://dx.doi.org/10.1088/1742-5468/acf8ba>.
- Malik Tiomoko, Romain Couillet, Eric Moisan, and Steeve Zozor. Improved estimation of the distance between covariance matrices. In *ICASSP 2019 - 2019 IEEE International Conference on Acoustics, Speech and Signal Processing (ICASSP)*, pages 7445–7449, 2019. doi: 10.1109/ICASSP.2019.8682621.
- Guodong Zhang, Chaoqi Wang, Bowen Xu, and Roger B. Grosse. Three mechanisms of weight decay regularization. *CoRR*, abs/1810.12281, 2018. URL <http://arxiv.org/abs/1810.12281>.
- Noam Levi and Yaron Oz. The underlying scaling laws and universal statistical structure of complex datasets. *arXiv preprint arXiv:2306.14975*, 2023a.
- Bruno Loureiro, Cedric Gerbelot, Hugo Cui, Sebastian Goldt, Florent Krzakala, Marc Mezard, and Lenka Zdeborova. Learning curves of generic features maps for realistic datasets with a teacher-student model. In *Advances in Neural Information Processing Systems*, volume 34, 2021d.
- Bruno Loureiro, Cedric Gerbelot, Hugo Cui, Sebastian Goldt, Florent Krzakala, Marc Mezard, and Lenka Zdeborova. Learning curves of generic features maps for realistic datasets with a teacher-student model. *Journal of Statistical Mechanics: Theory and Experiment*, 2022(11):114001, nov 2022. doi: 10.1088/1742-5468/ac9825. URL <https://doi.org/10.1088/1742-5468/ac9825>.
- Adityanarayanan Radhakrishnan, Mikhail Belkin, and Caroline Uhler. Wide and deep neural networks achieve consistency for classification. *Proceedings of the National Academy of Sciences*, 120(14), March 2023. ISSN 1091-6490. doi: 10.1073/pnas.2208779120. URL <http://dx.doi.org/10.1073/pnas.2208779120>.

- Kishore Jaganathan, Yonina C. Eldar, and Babak Hassibi. Phase retrieval: An overview of recent developments, 2015.
- Jonathan Dong, Lorenzo Valzania, Antoine Maillard, Thanh-an Pham, Sylvain Gigan, and Michael Unser. Phase retrieval: From computational imaging to machine learning: A tutorial. *IEEE Signal Processing Magazine*, 40(1):45–57, 2023. doi: 10.1109/MSP.2022.3219240.
- Emmanuel J. Candes, Xiaodong Li, and Mahdi Soltanolkotabi. Phase retrieval via wirtinger flow: Theory and algorithms. *CoRR*, abs/1407.1065, 2014. URL <http://arxiv.org/abs/1407.1065>.
- Yuxin Chen, Yuejie Chi, Jianqing Fan, and Cong Ma. Gradient descent with random initialization: fast global convergence for nonconvex phase retrieval. *Mathematical Programming*, 176(1–2): 5–37, February 2019. ISSN 1436-4646. doi: 10.1007/s10107-019-01363-6. URL <http://dx.doi.org/10.1007/s10107-019-01363-6>.
- Luca Arnaboldi, Florent Krzakala, Bruno Loureiro, and Ludovic Stephan. Escaping mediocrity: how two-layer networks learn hard generalized linear models with sgd, 2024.
- Simon Martin, Francis Bach, and Giulio Biroli. On the impact of overparameterization on the training of a shallow neural network in high dimensions, 2023.
- Roi Livni, Shai Shalev-Shwartz, and Ohad Shamir. On the computational efficiency of training neural networks, 2014.
- Mohammadreza Soltani and Chinmay Hegde. Towards provable learning of polynomial neural networks using low-rank matrix estimation. In Amos Storkey and Fernando Perez-Cruz, editors, *Proceedings of the Twenty-First International Conference on Artificial Intelligence and Statistics*, volume 84 of *Proceedings of Machine Learning Research*, pages 1417–1426. PMLR, 09–11 Apr 2018. URL <https://proceedings.mlr.press/v84/soltani18a.html>.
- Ziwei Ji and Matus Telgarsky. Directional convergence and alignment in deep learning, 2020.
- Kaifeng Lyu and Jian Li. Gradient descent maximizes the margin of homogeneous neural networks, 2020.
- Daniel Hsu, Vidya Muthukumar, and Ji Xu. On the proliferation of support vectors in high dimensions, 2022.
- Alex Krizhevsky. Learning multiple layers of features from tiny images. *University of Toronto*, 05 2012. URL <https://www.cs.toronto.edu/~kriz/learning-features-2009-TR.pdf>.
- Han Xiao, Kashif Rasul, and Roland Vollgraf. Fashion-mnist: A novel image dataset for benchmarking machine learning algorithms. *arXiv: 1708.07747*, 2017. doi: 10.48550/ARXIV.1708.07747.
- Kaiming He, Xiangyu Zhang, Shaoqing Ren, and Jian Sun. Deep residual learning for image recognition, 2015.
- Peter N. Belhumeur, João P. Hespanha, and David J. Kriegman. Eigenfaces vs. fisherfaces: Recognition using class specific linear projection. *IEEE Trans. Pattern Anal. Mach. Intell.*, 19(7):711–720, jul 1997. ISSN 0162-8828. doi: 10.1109/34.598228. URL <https://doi.org/10.1109/34.598228>.
- Noam Levi and Yaron Oz. The universal statistical structure and scaling laws of chaos and turbulence. *arXiv preprint arXiv:2311.01358*, 2023b.
- Vardan Pappayan, X. Y. Han, and David L. Donoho. Prevalence of neural collapse during the terminal phase of deep learning training. *Proceedings of the National Academy of Sciences*, 117(40): 24652–24663, September 2020. ISSN 1091-6490. doi: 10.1073/pnas.2015509117. URL <http://dx.doi.org/10.1073/pnas.2015509117>.

A Neural Collapse on Overlapping GMM Data

Here, we explore the concept of Neural Collapse (NC) on overlapping GMMs generated from real data. Practically, we employ the metrics given in Papayan et al. [2020] to measure the NC when training a ResNet18 on gaussian versions of CIFAR10 images. In Fig. 5, we show that NC occurs on overlapping GMMs even when the class mean vector of the data has been set to zero, indicating that expressive networks are able to perform nonlinear transformations that generate class means, where none were present, and at the final layer still perform linear classification.

Various metrics of Neural Collapse, as given by Papayan et al. [2020], are shown for GMMs generated from two classes of CIFAR10. Here, we use 5000 samples per class, training a ResNet18 to perform binary classification using cross-entropy loss, on GMMs generated from greyscale versions of CIFAR10 images. Each sample has dimension 1024, and the training is done using the default specifications provided in the supplementary code of Papayan et al. [2020]

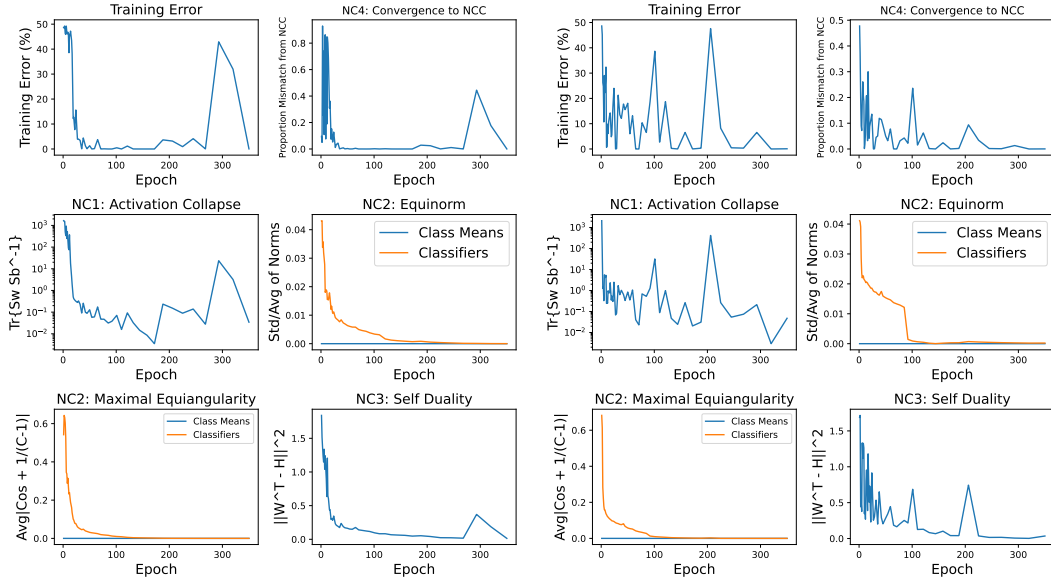


Figure 5: Results for neural collapse convergence for training ResNet18 on two classes (0,7) sampled from Gaussian versions of CIFAR10 data. Left: setting $\mu_A = \mu_B = 0$. Right: $\mu_A \neq \mu_B$, as given by the class means. The network attains 99.9% test accuracy in both cases. We see no substantial difference in convergence to neural collapse metrics, affirming our claims in the main text.

B KKT formulation

As discussed in the main text, we posit that the approach towards a BOC for a NN can be explained by convergence to a KKT point.

Our reasoning follows Theorem Theorem B.1 below, which holds for *gradient flow* (i.e., gradient descent with an infinitesimally small step size). Before stating the theorem, we need the following definitions: (1) We say that gradient flow *converges in direction* to $\tilde{\theta}$ if $\lim_{t \rightarrow \infty} \frac{\theta(t)}{\|\theta(t)\|} = \frac{\tilde{\theta}}{\|\tilde{\theta}\|}$, where $\theta(t)$ is the parameter vector at time t ; (2) We say that a network Φ is *homogeneous* w.r.t. the parameters θ if there exists $L > 0$ such that for every $\lambda > 0$ and θ, \mathbf{x} we have $\Phi(\alpha\theta; \mathbf{x}) = \lambda^L \Phi(\theta; \mathbf{x})$. Thus, scaling the parameters by any factor $\lambda > 0$ scales the outputs by λ^L . We note that essentially any fully-connected or convolutional neural network with ReLU activations is homogeneous w.r.t. the parameters θ if it does not have any skip-connections (i.e., residual connections) or bias terms, except possibly for the first layer.

Theorem B.1 (Paraphrased from Lyu and Li [2020], Ji and Telgarsky [2020]). *Let $\Phi(\theta; \cdot)$ be a homogeneous ReLU neural network. Consider minimizing the logistic loss over a binary classification*

dataset $\{(\mathbf{x}_a, y_a)\}_{a=1}^N$ using gradient flow. Assume that there exists time t_0 such that $\mathcal{L}(\boldsymbol{\theta}(t_0)) < 1^4$. Then, gradient flow converges in direction to a first order stationary point (KKT point) of the following maximum-margin problem:

$$\min_{\boldsymbol{\theta}'} \frac{1}{2} \|\boldsymbol{\theta}'\|^2 \quad \text{s.t.} \quad \forall i \in [n] \quad y_a \Phi(\boldsymbol{\theta}'; \mathbf{x}_a) \geq 1. \quad (19)$$

Moreover, $\mathcal{L}(\boldsymbol{\theta}(t)) \rightarrow 0$ as $t \rightarrow \infty$.

The above theorem guarantees directional convergence to a first order stationary point (of the optimization problem (Eq. (19))), which is also called *Karush–Kuhn–Tucker point*, or *KKT point* for short. The KKT approach allows inequality constraints, and is a generalization of the method of *Lagrange multipliers*, which allows only equality constraints.

The great virtue of Theorem B.1 is that it characterizes the *implicit bias* of gradient flow with the logistic loss for homogeneous networks. Namely, even though there are many possible directions of $\frac{\boldsymbol{\theta}}{\|\boldsymbol{\theta}\|}$ that classify the dataset correctly, gradient flow converges only to directions that are KKT points of Problem (Eq. (19)). In particular, if the trajectory $\boldsymbol{\theta}(t)$ of gradient flow under the regime of Theorem B.1 converges in direction to a KKT point $\tilde{\boldsymbol{\theta}}$, then we have the following: There exist $\lambda_1, \dots, \lambda_n \in \mathbb{R}$ such that

$$\tilde{\boldsymbol{\theta}} = \sum_{a=1}^N \lambda_a y_a \nabla_{\boldsymbol{\theta}} \Phi(\tilde{\boldsymbol{\theta}}; \mathbf{x}_a) \quad (\text{stationarity}) \quad (20)$$

$$\forall a \in [N], \quad y_a \Phi(\tilde{\boldsymbol{\theta}}; \mathbf{x}_a) \geq 1 \quad (\text{primal feasibility}) \quad (21)$$

$$\lambda_1, \dots, \lambda_N \geq 0 \quad (\text{dual feasibility}) \quad (22)$$

$$\forall a \in [N], \quad \lambda_a = 0 \text{ if } y_a \Phi(\tilde{\boldsymbol{\theta}}; \mathbf{x}_a) \neq 1 \quad (\text{complementary slackness}) \quad (23)$$

Our main insight is based on Eq. (20), which implies that the parameters $\tilde{\boldsymbol{\theta}}$ are a linear combinations of the derivatives of the network at the training data points. We say that a data point \mathbf{x}_a is *on the margin* if $y_a \Phi(\tilde{\boldsymbol{\theta}}; \mathbf{x}_a) = 1$ (i.e. $|\Phi(\tilde{\boldsymbol{\theta}}; \mathbf{x}_a)| = 1$). Note that Eq. (23) implies that only samples which are on the margin affect Eq. (20), since samples not on the margin have a coefficient $\lambda_a = 0$. In sufficiently high dimension we expect no samples to be off the margin in GMM classification therefore all λ_a should be nonzero and contribute a similar amount.

C Dataset Properties

We show the eigenvalues scaling structure and the Inverse Participation Ratio (IPR) of the eigenvectors. We separate the eigenvalues to three parts: I. The large eigenvalues, II. The bulk eigenvalues, and III. The small eigenvalues, as can be seen in Fig. 6. These three regimes are seen also in real datasets as shown in previous work [Levi and Oz, 2023a,b]. Fig. 6 shows the eigenvalues for each of the classes in the FMNIST and CIFAR10 datasets, respectively.

The IPR defined as:

$$IPR \equiv \left(\sum_n |v_n|^4 \right)^{-1}, \quad (24)$$

is used to measure the localization rate (entropy) of a vector. Fig. 7 shows the IPR of the eigenvectors of the covariance matrices for the different classes in the CIFAR10 dataset and FMNIST. As can be seen from the Figure, the changes in the eigenvalues structure and the IPR is small.

D Appendix - Flipping tests examples

We include the different figures concerning the classification flipping tests referred to in the main text. The diagram in Fig. 8 outlines the structure of the flipping tests. In Fig. 9 and Fig. 10 we see rotated images of FMNIST and CIFAR10, respectively. In Fig. 11, Fig. 12 and Figures 13 and 14 we plot the eigenvalues and eigenvectors thresholds.

⁴This ensures that $\ell(y_a \Phi(\boldsymbol{\theta}(t_0); \mathbf{x}_a)) < 1$ for all i , i.e. at some time Φ classifies every sample correctly.

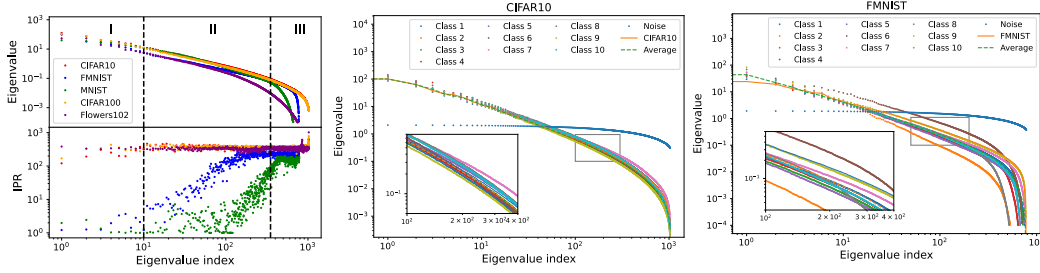


Figure 6: **Left:** Partition the eigenvector indices to three regimes: the large eigenvalues, the bulk and the small eigenvalues. The top figure shows the eigenvalues versus their index, and the bottom show the corresponding IPR versus the eigenvalues index. **Center/Right:** The eigenvalues of the covariance matrix for the different classes in CIFAR10/FMNIST dataset, with a comparison to uncorrelated data (**blue**). The **orange** line represents the eigenvalues of the covariance matrix of the whole dataset and the **green** dashed line shows the average of the different classes. We see the three regimes of eigenvalues: the large eigenvalues - up to ± 10 first eigenvalues, the bulk scaling - between ± 10 to ± 300 , and the small eigenvalues - from ± 350 .

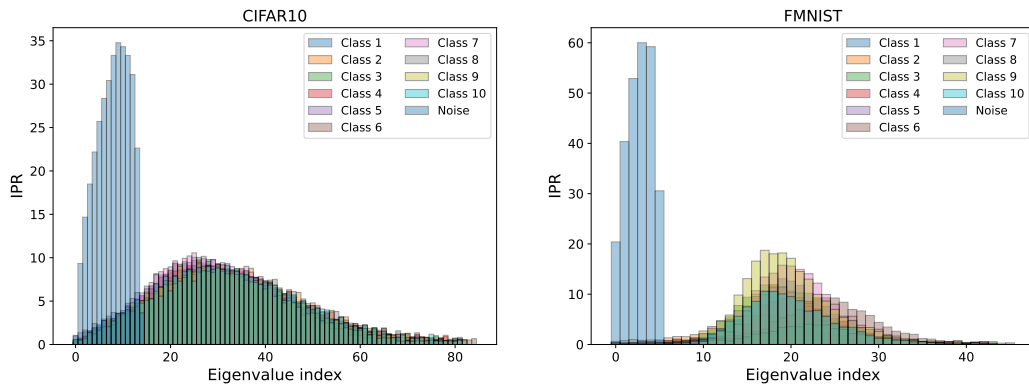


Figure 7: The histogram of the IPR of the covariance matrix eigenvectors for the different classes in the CIFAR10 dataset (left), and FMNIST (right), with a comparison to noise (blue).

The code for our experiments is provided in <https://github.com/khencohen/FlippingsTests>.

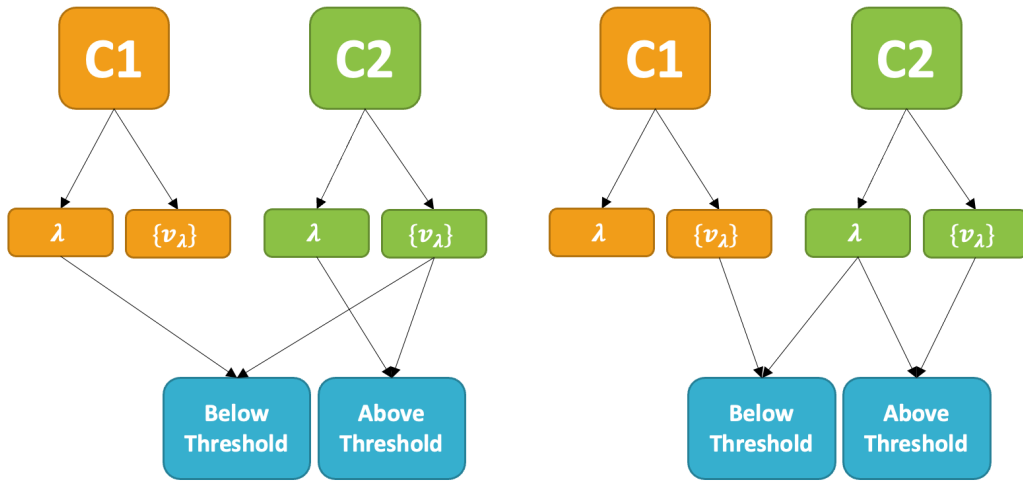


Figure 8: The classification flipping tests. We evaluate the model classification performance on different covariance matrices. Left - building a new covariance matrix by flipping the eigenvectors up to a certain threshold. Right - building a new covariance matrix by flipping the eigenvalues up to a certain threshold. This method provides information about the relative importance of the different eigenvectors and eigenvalues for the model to make a classification decision.

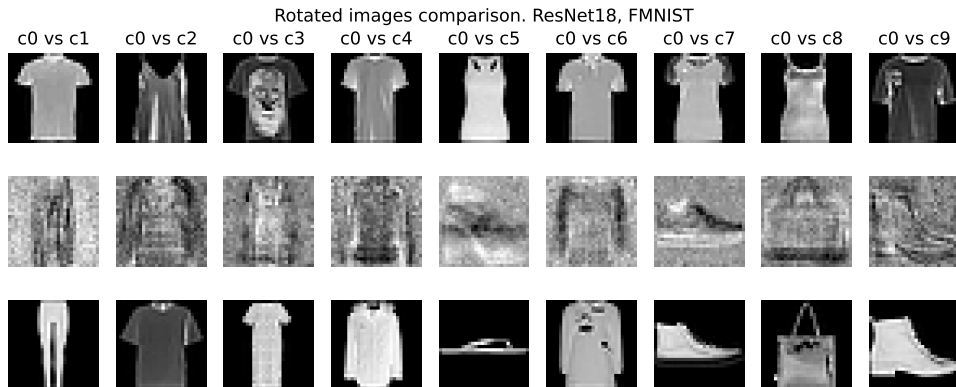


Figure 9: Examples of rotated images in the FMNIST dataset. Each of the samples of class 0 (shirt, top row), was rotated using the covariance matrix of another class (bottom row), and the middle row shows the result of the rotation. In all of our tests, for any rotation of class 0 sample, with class c basis, the model classified the rotated image as a sample from class c .

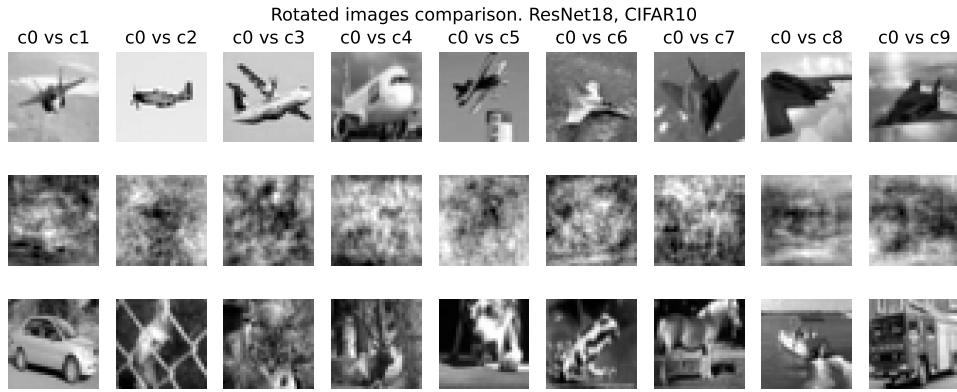


Figure 10: Examples of rotated images in the CIFAR dataset. Each of the samples of class 0 (airplane, top row), was rotated using the covariance matrix of another class (bottom row), and the middle row shows the result of the rotation. In all of our tests, for any rotation of class 0 sample, with class c basis, the model classified the rotated image as a sample from class c .

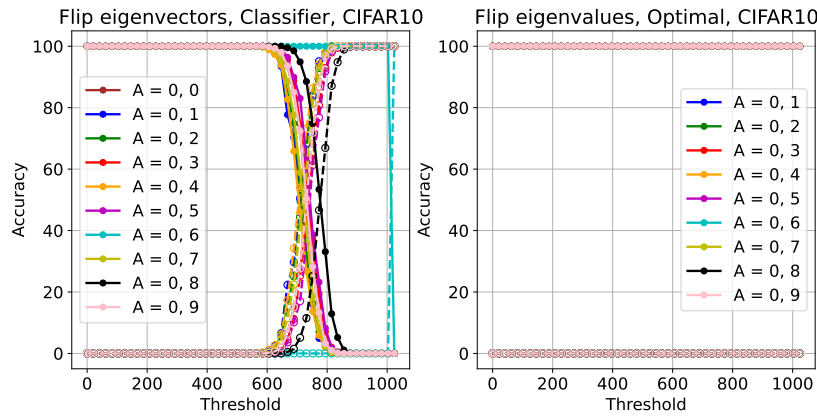


Figure 11: The classification eigenvector (left) and eigenvalues (right) flipping test on the optimal classifier. CIFAR10 dataset, comparing class 0 with other classes.

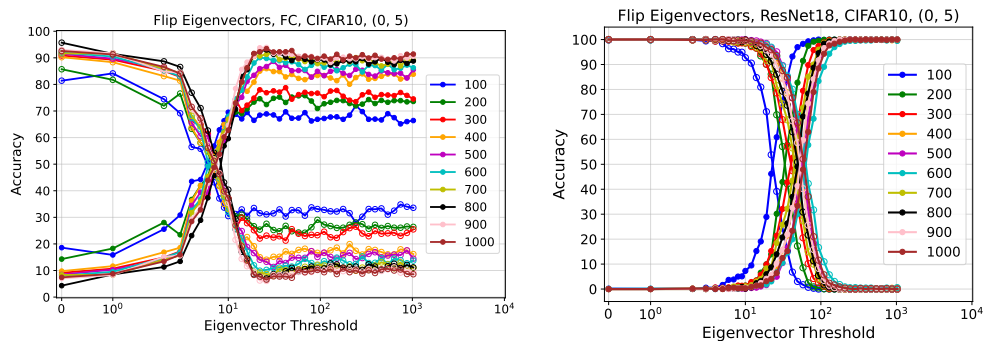


Figure 12: The classification eigenvector flipping test on the Gaussian dataset between class 0 and class 5, for different number of samples. FC model (left) and ResNet18 (right), CIFAR10 dataset.

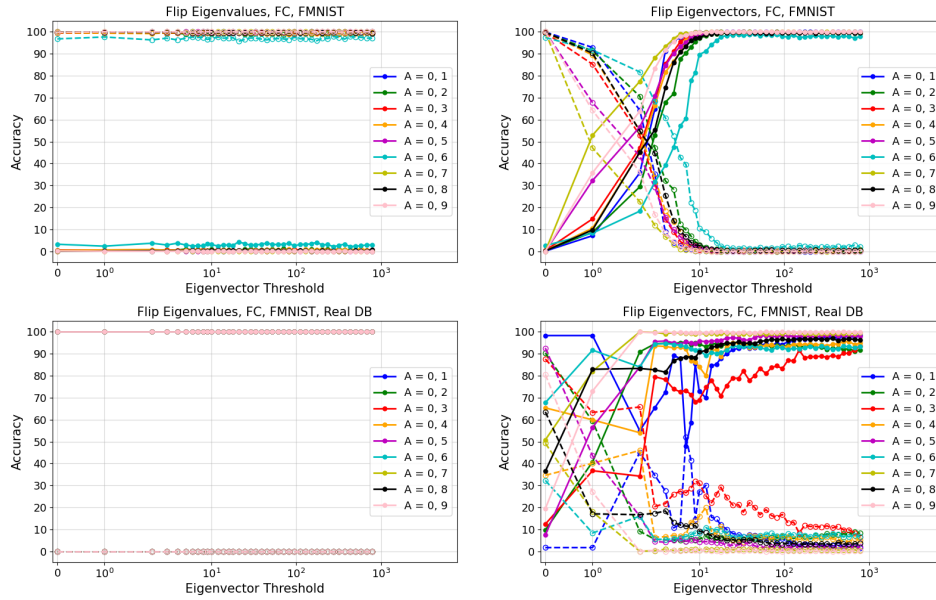


Figure 13: The classification eigenvalues flipping test on the rotated FMNIST dataset between class 0 and other classes for the FC model.

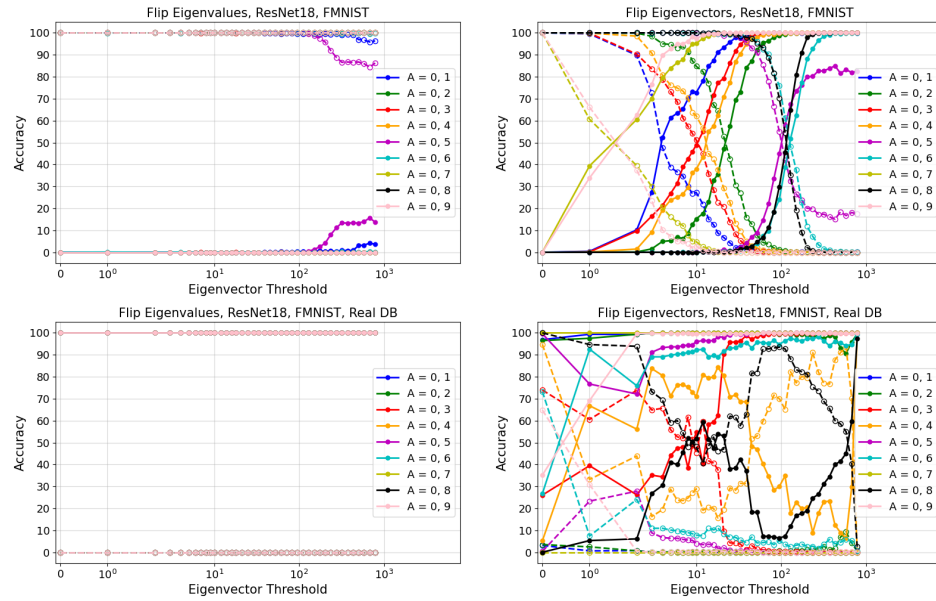


Figure 14: The classification eigenvalues flipping test on the rotated FMNIST dataset between class 0 and other classes for the ResNet 18 model.